GRAIN-ORIENTED SEGMENTATION OF SCANNING ELECTRON MICROSCOPE IMAGES

Hyun-Gyu Lee *Min-Kook Choi* *Sang-Chul Lee*

Department of Computer and Information Engineering, Inha University
{hg_lee, mkchoi, sclee}@inha.edu

ABSTRACT

Quantitative analysis of nanostructures from scanning electron microscope (SEM) images requires a clear segmentation of grains and their boundaries. This is not provided by active contour models, which also require user guidance. Our automatic technique creates a rough representation of grain boundaries by adaptive thresholding. It then performs ray-casting from a rectangular grid of seed points to ensure that the grain shapes are convex, and selects the best result for each grain. The whole process can be repeated several times to improve the segmentation. We present results for images of titanium foil, which show that our approach compares favorably in terms of speed and segmentation quality with four competing techniques.

Index Terms— Nanostructures, grain structure, image segmentation, anodization, Ti foil

1. INTRODUCTION

Nanostructured materials with discrete grains, such as block copolymer-derived nanowire arrays [1], block copolymers [2-4], nanospheres [5-7], are important due to their wide application [8]. Materials with a hexagonal grain structure have unique structural properties, allowing their use in catalysis, photonics, microelectronics and life sciences [8, 9].

Grain structure analysis is a key process in assessing the quality of the grain in self-assembled materials. Ideally, nanoporous materials have a uniform size of pore and a hexagonal lattice structure. Currently, it is labor-intensive to obtain this structural information. This has motivated research on the automatic determination of grain structures from SEM [16, 17] images. Global analysis of grain structure can be conducted in the signal processing domain using a 2D Fourier transformation which can determine the orientation distribution of hexagonal structures and average grain sizes. But such methods can only provide overall information about grain structures unless they are supported by the analysis of single grains and their local structures. Furthermore, these global analyses can be compromised by image defects caused by inhomogeneous contrast and blurred area.

To provide local structural information about single grain in the triangular and symmetric hexagonal structures of nanoporous alumina, Matefi-Tempfli et al. [10] suggested a method which finds repetitive shapes and the center of nanopores for local analysis. Hillebrand et al. [11] analyzed the properties of these grain structures. After identifying a single grain, they were able to determine nearest-neighbor distances, angles and grain sizes. Since this method uses information about a single grain obtained through regional analysis, it can cope with defective images to some extent. This approach has been extended in subsequent researches [12-15]. The local contrast in SEM images of nanoporous alumina typically varies between regions. A number of segmentation methods have been proposed to overcome this issue using techniques such as fuzzy thresholding using entropy [13] or adaptive thresholding based on histogram equalization [14, 15].

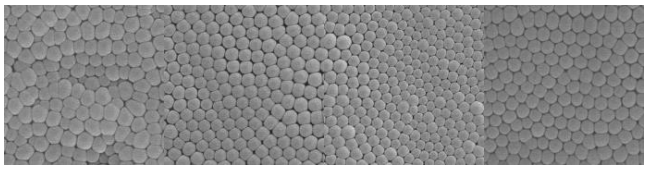

Fig. 1. The SEM images of titanium foil under various imaging conditions.

We propose a segmentation method for grain structure analysis of SEM images of titanium foil. This is challenging data, because it exhibits various imaging problems. Fig. 1 shows example SEM images of titanium foil. We overcome image defects by finding and repairing the boundaries of individual grains. We sample grain boundary using ray-casting and retain the best model of each grain. Their process can be applied iteratively to improve the segmentation. Our method can be used to improve the quantitative analysis of the self-ordered nanomaterials.

Our method consists of the following steps: (1) detect the boundaries of individual grains using a novel edge intensity description constraint (EIDC), (2) generate candidate grains by sampling their boundaries using ray-casting on a predetermined grid location, (3) cluster the seed points in candidate grains, and then select the best seeds based on a radius measurement of the boundary in each seed, (4) identify individual grains using the best seeds.

2. FINDING GRAIN BOUNDARIES

We need to approximate grains boundaries in an image to input into our ray-casting process. Standard edge-detectors perform poorly on SEM images due to variable intensity and irregular grain shapes. Fig. 2(b) and (c) show example results using the Sobel operator and Canny edge detector [18]. These techniques produce double edges due to the width of

the grain boundaries.

We pose edge detection as a process of discrimination between grain regions and edges. This is expressed as a maximization of the edge area while minimizing the area of each grain. We solve this problem by introducing an edge intensity description constraint (EIDC), which is an inequality constraint that satisfies two pre-defined conditions. The first condition is that the boundary of a grain has a lower intensity than the grain itself. The second condition is that the proportion of the area of an appropriately sized window occupied by grain edges is approximately the same. We can discriminate between edges and grains by thresholding a histogram of intensity within a window in a way that meets these two conditions. Problems can still occur with edges that are very thin or indistinct, but most edges have lower intensity than grains.

If $\mathcal{C}$ is a binary variable which indicates whether a pixel belongs to a grain (0) or an edge (1), then

$$\mathcal{C}(x,y) = \begin{cases} 1, & \alpha(x,y) < I(x,y) \\ 0, & \text{otherwise} \end{cases},$$

$$\alpha(x,y) = \underset{t}{\operatorname{argmin}} \left| \frac{1}{m^2} \left(\sum_{i=0}^{t} \sum_{u=-\frac{m}{2}}^{m/2} \sum_{v=-\frac{m}{2}}^{m/2} \Phi(x+u, y+v) \right) - \beta \right|,$$

$$\Phi(x+u,y+v) = \begin{cases} 1, & \text{if } I(x+u,y+v) = i \\ 0, & \text{otherwise} \end{cases}. \quad (1)$$

β is a threshold that determines the proportion of pixels belonging to edges in a $m \times m$ window size and $I(x,y)$ is the intensity of the pixel at (x,y). Using this formula, we build an edge map which is subsequently used as the basis for grain segmentation by boundary detection and reshaping. Fig. 2(d) shows the result of edge detection by EIDC.

3. GRAIN BOUNDARY ESTIMATION

After the segmentation process described in the previous section, some edges are incorrect because of closing or merging grains. Therefore, we apply a boundary estimation process which samples points on edges, generated the intersections of rays in the plane of the image from seed points, as shown in Fig. 3(a) and (b). Outlying intersections occur when edges are incomplete, and these must be eliminated (Fig.3(c)) to obtain an accurate grain area (Fig. 3(d)).

To exclude outlying intersections, we define the cost function as follows.

$$\Psi^* = \underset{\tilde{\Psi} \subseteq \Psi}{\operatorname{argmin}} \left\{ (1-\lambda) \sum_{i=1}^{k-1} \left| l_{i,\tilde{\Psi}} - l_{i+1,\tilde{\Psi}} \right| + \lambda(n-k) \right\}, (2)$$

where Ψ is the set of cast rays, Ψ^* is a subset of extending rays that satisfies the optimization condition, such that $\Psi^* \subseteq \Psi$, and $l_{i,\Psi}$ is the length of the ith ray that belongs to a candidate subset $\tilde{\Psi}$ that satisfies $l_{i,\tilde{\Psi}} \in \tilde{\Psi}$. The number of rays that belongs to Ψ is n, and k is the number of rays that belong to $\tilde{\Psi}$. The parameter λ adjusts the proportion of outlier intersections$(n-k)$. Optimization includes maximizing the number of rays of similar length.

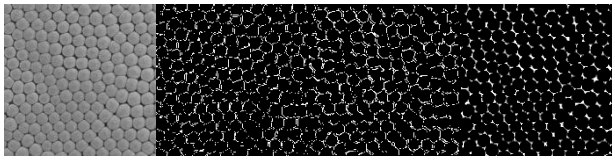

(a) (b) (c) (d)

Fig. 2. Edge detection using (b) the Sobel operator, (c) Canny edge detector and (d) EIDC in (a) an original image.

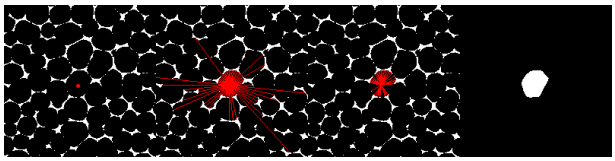

(a) (b) (c) (d)

Fig. 3. Grain segmentation based on ray-casting in the image plane: (a) seed point on a rough boundaries; (b) boundary sampling by ray-casting; (c) identifying inlier intersections by optimization; (d) final segmentation.

(a) (b) (c) (d)

Fig. 4. Boundary correction using CSC: (a) extended rays alone produce (b) a defective boundary; (c) extended rays satisfied by CSC produce (d) a convex boundary.

However, we cannot consider all combinations of inlier subsets, because of the computational complexity, which is $\sum_{k=1}^{n} n!/k!\,(n-k)!$, where n is the number of rays and k is the number of rays in a subset. We reduce this cost by reducing the number of candidate subsets. This approximation is achieved by considering the lengths of each ray. Inlier rays have a similar length, and outlier rays are shorter or longer than average length of inlier rays.

We therefore sort the rays with an ascending order of length, and assume that the inlier will be contiguous at the start of their list. By this approximation, the computational complexity of the optimization process is reduced to $O(n)$ by this approximation. Algorithm 1 shows boundary estimation. We simplify Eq. (2) by introducing the variable $\Delta L = \sum_{i}^{k-1} |l_i - l_{i+1}|$. $\mathcal{U}$ is the index of the ray of maximum length in the list of candidate inliers, and $\mathcal{L}$ indicates is the index of the ray of minimum length.

4. BOUNDARY CORRECTION AND BEST SEED SELECTION

We sow initial seeds at fixed intervals based on grid. Some are poorly located and generate distorted grain shapes. We therefore estimate the completeness of the grain boundary produced by each seed and eliminate these which produce very incomplete boundaries. We estimate the roundness R of a grain produced by a given seed as follows:

$$R = \frac{\sum \Gamma(x,y)}{A},$$

$$\Gamma(x,y) = \begin{cases} 1, \text{if } \sqrt{(x-p)^2 + (y-q)^2} < \tilde{r} \\ 0, \quad \text{otherwise} \end{cases}, \qquad (3)$$

where A is the area of the estimated grain in pixels, (p,q) are the coordinates of the center of the grain generated by boundary estimation, and (x,y) are the coordinates of a pixel in grain. The radius $\tilde{r}$ of the grain is $\sqrt{A/\pi}$. If the grain roundness R is lower than a threshold δ, the seed of the grain is discarded.

Even if the roundness R of a grain is high, the contour may not be convex. Fig. 4(a) and (b) show examples in which boundaries are generated non-convex boundaries due to the apparent merges of adjacent grains. We use a convex shape constraint (CSC) to ensure that grains are convex. Some outlier rays remaining after optimization are eliminated in this process.

The key idea of CSC is that the convexity of a polygon can be verified by finding a concave point which corresponds to a local minimum of the boundary curve such as Fig. 4(b), obtained from the second derivatives of neighboring rays. If the intersection created by a ray is a concave point, its relatively large second derivative is a local minimum among its neighboring points. In other words, the concave point ρ in the set of inlier rays Ψ^* corresponds to a local minimum of the ray lengths, and it can be detected by:

$$\nabla^2 f(s) = \lim_{\tau \to 0} \frac{f(s-\tau) - 2f(s) + f(s+\tau)}{\tau^2}, \qquad (4)$$

where f is a length from the center of the grain to the point of the boundary, s is the x-y position of a point corresponding to a ray, and τ is the x-y difference from the point to next point in the boundary direction. The CSC can then be calculated as follows:

$$l_\rho = l_i, \quad \text{if } l_{i-1} - 2l_i + l_{i+1} - \kappa > 0, \text{ s.t. } l_i \in \tilde{\Psi}, \qquad (5)$$

The final term κ is determined by the number of rays and normalized by the constant σ, s.t. $\kappa = \frac{n}{\sigma}$, and l_ρ is the ray corresponding to a concave point found in Ψ^*. In case of hexagon-shaped structures, since the concave points are usually detected in a pair, ρ_1 and ρ_2, we divide the detected regions into two separate sub-regions and discard the sub-region with smaller number of rays, by eliminating all the rays corresponding to the discarded sub-area.

Finally, we cluster seeds on the basis of their radius $\tilde{\boldsymbol{r}}$. We merge seeds with overlapping radii $\tilde{\boldsymbol{r}}$ into clusters. In each cluster, the seed with the highest roundness $\boldsymbol{R}$ is selected, and the remainders are discarded.

Although our method is aimed to detect grain boundary under thin and indistinct edge conditions, grains may not be found when boundaries in edge map is very poor. To overcome this problem, we repeatedly apply this process (section 2-4) separately to repair the edge map until no more grains are newly found. Because convex boundaries of grains estimated by the process update to edge map, our method iteratively builds edge map more clearly (see Fig. 7).

Algorithm 1 Estimating approximate grain boundary

procedure Given a set of rays Ψ
***Variable description and initialization*:**
l_i: i −th ray belong to Ψ
$\tilde{l}_i$: i −th ray that is sorted by ascending order of l_i
$\Upsilon \leftarrow \infty$: temporary variable
***Finding the inlier of maximum length*:**
for $m \leftarrow 2,\ n-1$ **do**
$\widetilde{\Delta L} = \sum_{j=1}^{m} \tilde{l}_j - \tilde{l}_{j+1}$
if $\Upsilon > (1-\lambda)\widetilde{\Delta L} + \lambda(n-k)$
then $\Upsilon \leftarrow (1-\lambda)\widetilde{\Delta L} + \lambda(n-k),\ \mathcal{U} = m$
end for
***Variable initialization*:** $\Upsilon \leftarrow \infty$
***Finding the inlier of minimum length*:**
for $m \leftarrow 1,\ \mathcal{U}$ **do**
$\widetilde{\Delta L} = \sum_{j=m}^{\mathcal{U}} \tilde{l}_j - \tilde{l}_{j+1}$
if $\Upsilon > (1-\lambda)\widetilde{\Delta L} + \lambda(n-k)$
then $\Upsilon \leftarrow (1-\lambda)\widetilde{\Delta L} + \lambda(n-k),\ \mathcal{L} = m$
end for
***Building the set of inliers*:**
Set $\tilde{l}_\chi \in \Psi^*, \chi = \{\mathcal{L}, \mathcal{L}+1, \dots, \mathcal{U}-1, \mathcal{U}\}$
return Ψ^*
end procedure

5. EXPERIMENTAL RESULTS

We used our technique to segment 14 SEM images of titanium foil. All the experiments were performed on a PC with an Intel i7 CPU 2.80GHz with 8GB of memory. Fig. 5 shows that initial edges become stable after sufficiently large window, e.g., 30 by 30 in our example. For a single grain detection, we compared our method with four state-of-the-art active contour model techniques in terms of initialization requirements, computation time, and segmentation results of 6 example grains, using an error ϵ metric, defined as follows:

$$\epsilon = 1 - \frac{TP + TN}{(TP + TN + FP + FN)}, \qquad (6)$$

where TP, FP, TN and FN are the true-positive, false-positive, true-negative and false-negative rates, respectively. The green lines in Table 1 are manually input approximation of a grain boundary. Although all active contour model (ACM)-based require this input, they produce the unacceptable segmentation results, drown by yellow lines. Mile's [21] and Bernard's [22] methods identified unexpected regions unrelated to the manual input. Other methods [19, 20] didn't detect the grain edges very accurately, but made them too small as too large. Shemesh's [19] technique produced the best results among ACM-based methods. Still, our technique found the grain boundary more accurately and ran faster than the other methods. Segmentation results for different numbers of iterations are shown in Fig. 7. The grains found in each iteration are used to repair the edge map in the next iterations, and so more iteration produces a better seg-

mentation. Fig. 6 shows the segmentation achieved with selected parameters when iteration converges. Note that to apply the method to all the datasets, only one set of parameters are selected based on 14 different datasets that contain various cell sizes, illuminations, edge thicknesses, and cell roundness. Each color in a grain represents each label of a grain. It shows our method precisely detected almost all grains which present large variations in sizes, shapes and intensities, and achieved very accurate segmentation result.

6. CONCLUSIONS

We have proposed a novel method of segmenting SEM images by ray-casting, which requires no initialization. It uses the new estimation metrics EDIC, CSC, and the roundness of a grain. Our method detects grain boundaries at least as accurately as competing methods, but requires no initialization. Others techniques are generally designed for SEM images of particular materials, or images with distinct edge, but our method can segment the grain structure in an entire image.

We expect the more meaningful quantitative analysis of grain morphology in hexagonal lattices structure for further researches, and this method can be applied to automatically quantifying ordering scores by anodizing. In future research, we aim to improve our method by introducing a more robust technique for blurred areas.

7. ACKNOWLEDGEMENTS

This research was supported by Next-Generation Information Computing Development Program through the National Research Foundation of Korea(NRF) funded by the Ministry of Education, Science and Technology (No. 2012M3C4A7032781). This research was supported by Basic Science Research Program through the National Research Foundation of Korea (NRF) funded by the Ministry of Education, Science, and Technology (No. 2012R1A1A1044658).

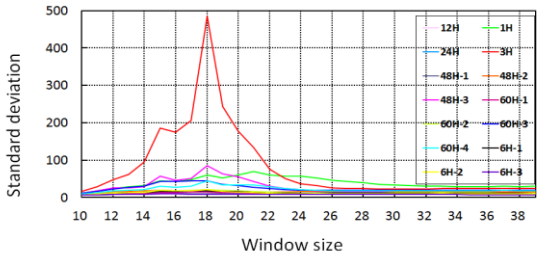

Fig. 5. Standard deviations of edge fragment sizes obtained by window sizes in 14 datasets (each set acquired based on different manufacturing durations, 1 hour to 60 hours).

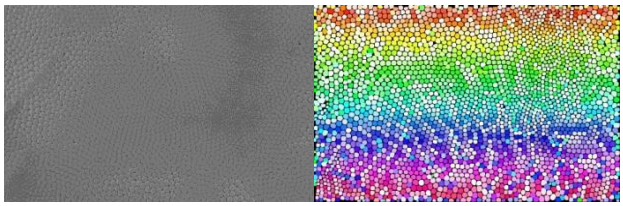

Fig. 6. A segmentation after several iteration with the selected parameters: $\beta = 0.06$, $\delta = 0.79$, $\sigma = 0.055$, and $\lambda = 0.96$, also used for final results in Fig. 6 and Table 1.

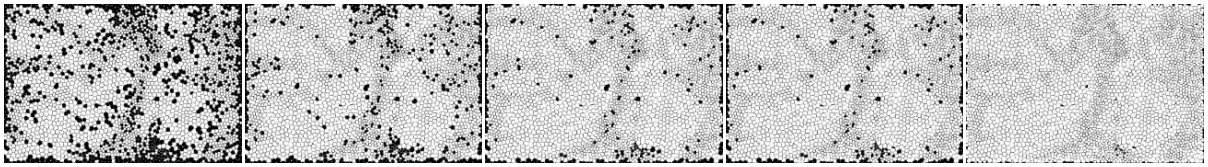

Fig. 7. A segmentation improved by iterations to repair boundaries in fixed parameters. From left to right: 1, 3, 5, 7 and 17 iterations.

Table 1. Comparison of our method with four other interactive segmentation techniques. For demonstration purpose, we sampled 6 grains particularly with irregular shapes, sizes, and illuminations from 14 different datasets.

Method	Initialization	Comp. Time (Sec)	grain 1	grain 2	grain 3	grain 4	grain 5	grain 6	Ave. ϵ
Proposed	Not required	**1.091**							**0.021**
Shemesh [19]	Required	1.124							0.036
Li [20]	Required	2.325							0.046
Mile [21]	Required	2.276							0.374
Bernard [22]	Required	5.575							0.635

8. REFERENCES

[1] D. Zschech, D.H. Kim, A.P. Milenin, R. Scholz, R. Hillebrand, C.J. Hawker, T.P. Russell, M. Steinhart and U. Gosele , "Ordered arrays of <100>-oriented silicon nanorods by CMOS-compatible block copolymer lithography". Nano Lett., vol. 7, no. 6, pp. 1516-1520, 2007.

[2] F. S. Bates and G. H. Fredrickson, "Block copolymer thermodynamics-theory and experiment", Annu. Rev. Phys. Chem., vol. 41, pp. 525-557, 1990.

[3] V. Castelletto and I. W. Hamley, "Morphologies of block copolymer melts", Curr. Opin. Solid State Mater. Sci., vol. 8, no. 6, pp. 426-438, 2004.

[4] V. Abetz and P. F. W. Simon, "Phase behavior and morphologies of block copolymers", Adv. Polym. Sci., vol. 189, pp. 125-212, 2005.

[5] C. B. Murray, C. R. Kagan and M. G. Bawendi, "Self-organization of CdSe nanocrystals into 3-dimensional quantum dot superlattices", Science, vol. 270, no 24, pp. 1335-1338, 1995.

[6] C. B. Murray, C. R. Kagan and M. G. Bawendi, "Synthesis and characterization of monodisperse nanocrystals and close-packed nanocrystal assemblies", Annu. Rev. Mater. Sci., vol. 30, pp. 545-610, 2000.

[7] P. Pieranski, "Colloidal Crystals", Contemp. Phys., vol. 24, no. 1, pp. 25-73, 1983.

[8] M. L. K. Hoa, M. Lu and Y. Zhang, "Preparation of porous materials with ordered hole structure", Adv. Colloid Interface Sci., vol. 121, no. 1-3, pp. 9-23, 2006.

[9] J. Wijnhoven and W. L. Vos, "Preparation of photonic crystals made of air spheres in titania", Science, vol. 281, no. 5378, pp. 802-804, 1998.

[10] S. Matefi-Tempfli, M. Matefi-Tempfli and L. Piraux, "Characterization of nanopores ordering in anodic alumina", Thin Solid Films, vol. 516, no. 12, pp. 3735-3740, 2008.

[11] R Hillebrand, F Muller, K Schwirn, W Lee and M Steinhart, "Quantitative analysis of the grain morphology in self-assembled hexagonal lattices", ACS Nano, vol. 2, no. 5, pp. 913-920, 2008.

[12] M. Abdollahifard, K. Faez, M. Pourfard and M. Abdollahi, "A histogram-based segmentation method for characterization of self-assembled hexagonal lattices", Appl. Surf. Sci., vol. 257, no. 24, pp. 10443-10450, 2011.

[13] M. Pourfard and K. Faez, "A statistical approach for the characterization of self-assembled hexagonal lattices", Appl. Surf. Sci., vol. 259, no. 15, pp. 124-134, 2012.

[14] J. R. Borba, C. Brito, P. Migowski, T. B. Vale, D. A. Stariolo, S. R. Teixeira and A. F. Feil, "Quantitative characterization of hexagonal packings in nanoporous alumina arrays: a case study", J. Phys. Chem., vol. 117, no. 1, pp. 246-251, 2013.

[15] N. Winkler, J. Leuthold, Y. Lei and G. Wilde, "Large-scale highly ordered arrays of freestanding magnetic nanowires", J. Mater. Chem., vol. 22, no. 32, pp. 16627-16632, 2012.

[16] D. McMullan, "Scanning electron microscopy 1928–1965". Scanning, vol. 17, no. 3, pp. 175-185, 1995.

[17] D. McMullan, "Von Ardenne and the scanning electron microscope", Proc. Roy. Microsc. Soc., vol. 23, pp. 283-288, 1988.

[18] J. Canny, "A computational approach to edge detection", IEEE Trans. Pattern Analysis and Machine Intelligence, vol. 8, no. 6, pp. 679-698, 1986.

[19] M. Shemesh and O. Ben-Shahar, "Free boundary conditions active contours with applications for vision", Advances in Visual Computing, vol. 6938, pp. 180-191, 2011.

[20] C. Li, C. Xu, C. Gui, and M. D. Fox, "Distance regularized level set evolution and its application to image segmentation", IEEE Trans. Image Process., vol. 19, no. 12, pp. 3243-3254, 2010.

[21] J. Mille, "Narrow band region-based active contours and surfaces for 2D and 3D segmentation", Computer Vision and Image Understanding, vol. 113, no 9, pp. 946-965, 2009.

[22] O. Bernard, D. Friboulet, P. Thevenaz and M. Unser. "Variational B-spline level-set: a linear filtering approach for fast deformable model evolution". IEEE Trans. Image Process., vol. 18, no. 6, pp. 1179-1191, 2009.